Biomaterials Advances 135 (2022) 112669

Contents lists available at ScienceDirect

Biomaterials Advances

journal homepage: www.elsevier.com/locate/bioadv

Microfibrillated cellulose-enhanced carboxymethyl chitosan/oxidized starch sponge for chronic diabetic wound repair

Lin-yu Long [a,1], Cheng Hu [a,1], Wenqi Liu [a], Can Wu [a], Lu Lu [b], Li Yang [a,*], Yun-bing Wang [a]

[a] National Engineering Research Center for Biomaterials, Chuanda-Jinbo Joint Research Center, Sichuan University, Chengdu 610064, China
[b] Key Laboratory of Medical Molecular Virology (MOE/NHC/CAMS), School of Basic Medical Sciences and Shanghai Public Health Clinical Center, Fudan-Jinbo Joint Research Center, Fudan University, Shanghai 200302, China

ARTICLE INFO

Keywords:
Wound dressing
Hemostasis
Shape memory material
Anti-inflammation
Angiogenesis

ABSTRACT

Herein, a novel microfibrillated cellulose (MFC) reinforced natural polymer-based sponge composed of carboxymethyl chitosan (CMC) and oxidized starch (OS) with hemostatic, repairing-promoting, and antimicrobial performances was fabricated for chronic wound repair. When the content of MFC reached 1.2 wt%, the prepared sponge exhibited ultra-fast water or blood-trigged shape recovery property within 3 s. Moreover, sponge was functionally modified with silver nanoparticles (AgNPs) and recombinant humanized collagen type III (rhCol III). The AgNPs and rhCol III loaded sponge (A-Ag/III) could effectively kill a broad spectrum of pathogenic microbes, promote the proliferation and migration of L929 cells *in vitro*. Due to their erythrocyte-aggregating ability and positive-charge feature of CMC, the A-Ag/III displayed rapid hemostasis ability. Furthermore, the *in vivo* animal experiment demonstrated the A-Ag/III could promote wound repair by inhibiting inflammation, promoting angiogenesis, and cell proliferation.

1. Introduction

Uncontrolled bleeding or massive hemorrhage caused by trauma is the leading reason for morbidity and mortality, occupying more than a quarter of all trauma deaths [1–3]. For the survival and optimal recovery of major trauma, early intervention to stanch bleeding is critical [4,5]. The existing hemostatic treatment in standard care usually relies on compressed cloth or gauze which can effectively stop bleeding [6]. However, for the deep, narrow, irregular, and incompressible damage caused by bullets, bombs, and explosives in the battlefield or daily life, the therapeutic effects of traditional hemostatic materials are somewhat unsatisfactory [2,7]. Considering the complicated physiological environment and healing process of the chronic wound [8,9], various advanced hemostatic materials can not only promote more effective and rapid hemostasis, but also possess some attractive functions of inhibiting infection of full-thickness wounds [10,11], facilitating angiogenesis [12], and promoting complex tissue regeneration processes [8] have been developed. However, although some gratifying progress has been achieved, it is still a challenge for the fabrication of multi-functionalize hemostatic materials to promote the repair of chronic wounds without affecting its hemostatic performance.

The present primary categories of hemostatic materials involve gauze, powder, hydrogel, and sponge which are usually fabricated from absorbable gelatin, modified collagen, thrombin, and calcium alginate [13–15]. However, owing to the poor availability, high cost, and infection issues, the clinical application of these products has been greatly restricted [16]. Currently, chitosan (CS), carboxymethyl chitosan (CMC), and other chitosan-based derivates have attracted attention in the hemostatic area due to their biocompatibility, biodegradability, hydrophilicity, and air permeability [7,15,17–22]. CS is a bioactive polymer and produced from the chitin that exists in crab, fungi, shrimp, insects, algae and bacterial cell walls by alkaline deacetylation process [23–25]. And for the purpose of achieving better therapeutic effects, a wide range of chitosan derivatives with excellent properties (for example, increased solubility, antibacterial activity, cell uptake, pH sensitivity, anti-oxidation and cell targeting capabilities) have been produced through chemical or enzymatic modification [26–31]. In addition, after contacting with blood, the $-NH_2$ on the CS molecular chain will be protonated to $-NH_3^+$, and then electrostatically interact with the negatively charged cell membrane of erythrocyte, causing erythrocyte adhesion and aggregation at the wound site, and eventually developing a blood clot [15,20,32–34]. In particular, CS-based sponge with large surface area and porous structure can aggregate blood cells and platelets to stop bleeding quickly, making it a powerful candidate for bleeding control [6,15]. However, the poor mechanical performance and unstable chemical properties of CS-based sponges limit their further clinical application in uncontrolled massive bleeding like arterial injury, or narrow deep non-compressible bleeding such as gunshot wounds [35].

To solve these above problems, the microfibrillated cellulose (MFC) was introduced to enhance the CMC-based sponge, which was fabricated by cross-linking oxidized starch (OS) with CMC *via* the Schiff-base chemistry reaction. Due to its excellent mechanical strength, high aspect ratio (fiber

* Corresponding author.
E-mail address: yanglisc@scu.edu.cn (L. Yang).
[1] These authors contributed equally to this work.

http://dx.doi.org/10.1016/j.msec.2022.112669
Received 24 November 2021; Received in revised form 3 January 2022; Accepted 15 January 2022
Available online 24 January 2022

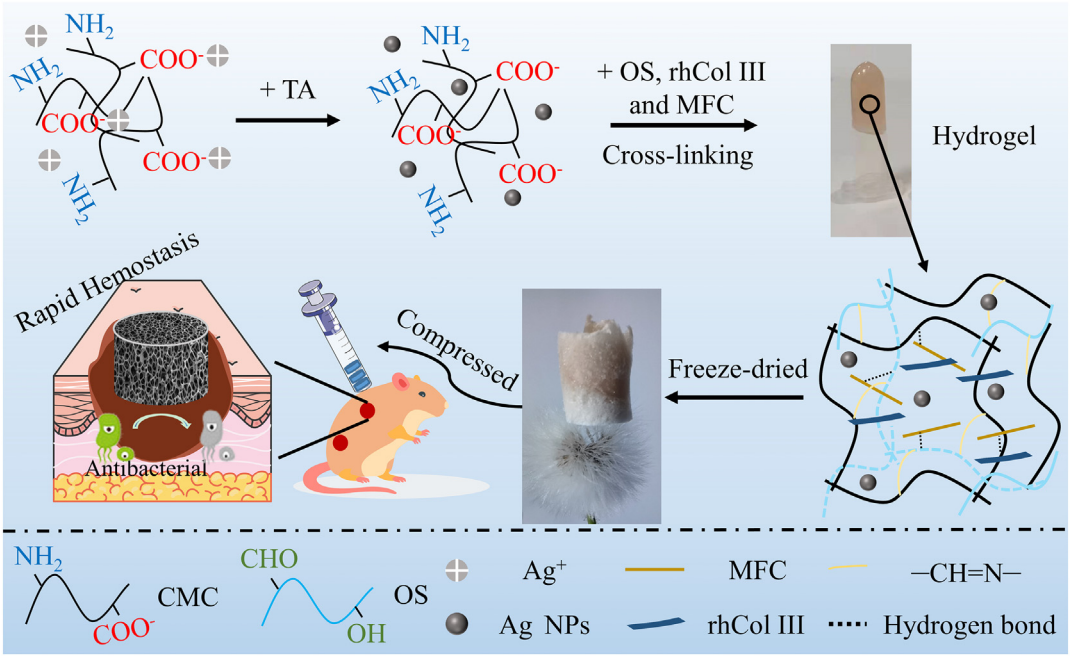

Fig. 1. Schematic presentation of the preparation of the injectable, antibacterial, and fast hemostatic MFC-reinforced CMC/OS sponge for chronic wound repair.

diameter less than 100 nm and length of several microns), and biodegradability, MFC has been extensively applied to reinforce a variety of materials [36–40]. Herein, it was assumed that after a certain amount of MFC was added, the CMC/OS sponge could be given excellent water/blood trigger shape recovery ability. As shown in Fig. 1, the CMC/OS-MFC sponge was further loaded with silver nanoparticles (AgNPs) and recombinant humanized collagen type III (rhCol III). The rhCol III used in this paper possessed strong cell adhesion and was synthesized based on the Gly483-Pro512 segment, which contained the highly adhesive fragments (GER, GEK), in the human collagen type III sequence [41]. First, the ability of the prepared sponge to promote cell migration and proliferation, as well as its antibacterial effects against *S. aureus* and *E. coli* were evaluated in this paper. And the porous shape-memory sponges with tough mechanical strength could be injected to narrow and deep wounds *via* a medical syringe after being compressed. Once the compressed sponges contacting blood, they could quickly recover their original shape to form a physical barrier and further stop blood loss. And the water/blood trigger shape recovery ability and hemostatic property of the prepared sponge were also assessed. In addition, a diabetic rat infected full-thickness skin wound model was used to verify the performance of the prepared sponge to accelerate wound repair.

2. Materials and methods

2.1. Materials

CMC (degree of carboxylation ≥80%) was purchased from Shanghai Macklin Biochemical Co., Ltd. (Shanghai, China); Starch soluble, tannic acid (TA), silver nitrate, and sodium periodate were purchased from Shanghai Titan scientific Co., Ltd. (Shanghai, China); MFC suspension (1.7 wt%, diameter: 0.1–1.0 μm; length: >20 μm) was purchased from Guilin Qihong Technology Co., Ltd. (Guilin, China); rhCol III was prepared by Shanxi Jinbo Bio-Pharmaceutical Co., Ltd. (Taiyuan, China). rhCol III is composed of 16 tandem repeats of the triple-helix fragment. The tandem repeats peptide contains the sequence of high cytoactive, derived from the Gly483-Pro512 sequence of the human type III collagen [41].

2.2. Preparation of oxidized starch (OS)

The OS was prepared by oxidizing starch with $NaIO_4$. In short, soluble starch (1 g, 2% w/v) was dissolved in certain distilled water, and 10 ml of $NaIO_4$ solution (5 wt%) was added dropwise into the mixture. Then the mixture was further stirred in the dark for 12 h at room temperature (RT). Finally, 2 ml of ethylene glycol was added to stop the reaction and dialyzed against water for 5 days. The OS was obtained by freeze-drying for 3 days.

2.3. Fabrication of the CMC/OS sponge with different MFC concentration

The CMC/OS-MFC sponge was prepared by a simple two-step method including the sol-gel process and freeze-drying. Firstly, 0.25 ml of MFC suspension with different mass fractions were mixed with 0.25 ml of CMC solution (10 wt%), followed by mixing with 0.5 ml of the OS solution (5 wt%). Then the mixture was poured into the mold and stand for 30 min until a stable hydrogel was formed. And the CMC/OS-MFC sponge was obtained by freeze-drying for 48 h. According to the initial concentration of MFC (0, 0.2, 0.4, 1.2 wt%), the sponges were named as CMC/OS-MFC_0, CMC/OS-$MFC_{0.2}$, CMC/OS-$MFC_{0.4}$, CMC/OS-$MFC_{1.2}$.

2.4. Fabrication of the Ag nanoparticles (AgNPs) and rhCol III decorated CMC/OS-MFC sponge

The AgNPs and rhCol III decorated CMC/OS-MFC sponge was prepared as shown in Fig. 1. Here, TA was used to reduce silver ions in CMC solution. 30 μg of $AgNO_3$ was added into 0.25 ml of CMC solution (10 wt%), 3 μg of TA was added after stirring for 0.5 h. And the antibacterial hemostatic sponge was prepared by the method described in Section 2.3. According to the addition of AgNps or rhCol III, the sponges were named A-C, A-Ag, A-III, and A-Ag/III.

2.5. Structure characterization

Scanning electron microscopy (SEM, S4800, Hitachi, Japan) was used to observe the morphologies of the freeze-dried sponges; Fourier transform infrared spectrometer (FT-IR, Nicolet iN10, Thermofisher Scientific, China) and X-ray diffraction spectrometer (XRD, D8 advance, Bruker, Germany) were used to analyze the chemical structure and crystals of the sponges, respectively. And the thermal stability of the materials was investigated by using the thermogravimetric analyzer (TGA) (SDT-Q600, TA Instruments, America) from the room temperature to 800 °C under N_2 atmosphere at 10 °C/min heating rate.

The swelling ratio of sponges in deionized water (DI) water was tested at RT. The freeze-dried sponges were firstly weighed (W_0). Then, they were swollen in DI water for 30 s and weighed again (Ws). The swelling ratio (SR) was calculated as.

$$SR = (Ws - W_0)/W_0 \times 100\%$$

2.6. Mechanical performance

The mechanical performance of the sponges was evaluated by compression test using the universal testing machine (BioTester, CellScale, Waterloo, Ontario, Canada) at RT. The sponges were first cut into cylinders with a diameter and height of 10 mm. The compression test was carried out for 60 s, and the maximum compressive strain was 80%.

In addition, the cyclic compression test of the swollen sponges was used to investigate the structural stability of the swollen sponges. The swollen sponges were performed up to 80% strain and then returned to the initial strain. This compression test was repeated 5 times.

2.7. Ag^+ and rhCol III release of sponges

For the cumulative Ag^+ release, the sponges were immersed into certain amount of PBS solution (10 ml, pH = 7.4) and kept at 37 °C. At the selected time, 0.5 mL of PBS was taken out to detect the silver content by using an inductively coupled plasma optical emission spectrometer (ICP-OES), and 0.5 mL of fresh PBS solution was added.

For the cumulative rhCol III release, the rhCol III was first labeled by fluorescein isothiocyanate (FITC). Then the FTIC labeled rhCol III loaded sponges were immersed into PBS solution (10 ml, pH = 7.4) at 37 °C. At the set time, 0.5 mL of PBS was taken out to detect the released FTIC labeled rhCol III by using a fluorescence spectrophotometer (Fluoroskan, Thermofisher Scientific, China), and 0.5 ml fresh PBS solution was replenished.

2.8. Hemolytic activity assay of the sponges

The hemolytic assay was conducted to investigate the biocompatibility of the prepared sponges in wound-care applications. Blood from SD rat was collected and the erythrocytes were obtained by centrifuged at 1500 rpm for 10 min. The erythrocytes were repeatedly washed with PBS for 3 times, and then diluted with PBS at a ratio of 1:9. Subsequently, the dried sponges were incubated in erythrocyte suspension for 1 h at 37 °C. And an UV–vis was used to detect the absorption peak of the supernatant after centrifugation at 540 nm to evaluate the hemolysis of the sponge. The positive (At) and negative (Ab) controls were 1% Triton-X and PBS, respectively. The sponges' hemolysis percentage was determined by using the following formula:

$$\text{Hemolysis } (\%) = [(An - Ab)/(At - Ab)] \times 100\%$$

2.9. In vitro degradation behavior

In vitro degradation experiments were carried out in a simulated physiological environment. In brief, pre-weighted sponges (W_0) were immersed in PBS (10 ml, pH = 7.4) at 37 °C and shaken at 60 rpm. At the set time (5, 10, 15, 20, 25, 30 d), sponges were taken out and then weighed after lyophilization (W_t). And the weight loss percentage (ΔW%) of sponges was determined according to the following formula:

$$\Delta W\% = (W_0 - W_t)/W_0 \times 100\%$$

2.10. Sponges' biocompatibility studies

The CCK8 experiment was used to evaluate the sponges' biocompatibility by co-cultivating L929 cells and sponges extract solution. The dried sponges were immersed into 5 mL complete 1640 cell medium and shaken at 100 rpm for 24 h to prepare the sponge extract solution. The culture medium of L929 cells was replaced with sponges extract solution and then cells were cultured at 37 °C (5% CO_2). After 24 h and 48 h, the CCK8 experiment was conducted to determine the cell viability (%). Each experiment was performed six times. In addition, FDA (50 μg/mL) was used to stain L929 cells to observe cells proliferation and morphology.

2.11. Cell scratch experiment

The cell scratch experiment was used to assess the influence of sponges on cell migration. Briefly, L929 cells were seeded in 6-well plates at rate of 1×10^6 and incubated at 37 °C for 24 h. After scratching the wells with a 200 μL pipette tip, the cell culture medium was replaced with sponges extract and incubated at 37 °C (5% CO_2). The microscopic images were taken immediately at the set time. Each experiment was performed three times, and representative images were selected.

2.12. In vitro antibacterial experiments

The antibacterial activity of A-C, A-Ag, A-III, and A-Ag/III was conducted using *S. aureus* and *E. col.* For bacterial optical density detection, sterilized sponges were added to the bacterial suspension. After incubating for a certain period of time, the density of the bacteria was determined by detecting the optical density (OD) at 600 nm. All of the experiments were performed in triplicate to confirm reproducibility. And the bacterial live and dead assay was carried out to confirm the influence of the prepared sponges on behaviors of bacterial death. The bacteria suspension was incubated with sterilized sponges in a constant temperature incubator (37 °C, 12 h), then the mixture was stained with SYTO 9 and propidium iodide (PI) and imaged with fluorescence microscopy. For the zone of inhibition assay, bacterial suspension (10^5–10^6 CFU/mL) was inoculated on the surface of the bacterial culture plate. The sponges were adhered to the culture plate and cultured upside down for 24 h at 37 °C to observe antibacterial effect of sponges.

2.13. Whole-blood clotting of the sponges

In Brief, 50 μL of fresh activated blood from SD rat was dripped onto the surface of sponge and incubated at 37 °C for 1 h. At 10 min intervals, 2.5 mL of distilled water was added and incubated for another 5 min. Then the hemoglobin concentration was evaluated by measuring the relative absorbance at 545 nm using a UV spectrophotometer.

2.14. Blood cells and platelet adhesion

The whole blood was centrifuged at the speed of 1500 r/min for 15 min to obtain the platelet-rich plasma. And the fresh platelet-rich plasma was dripped onto the surface of sponges and further incubated at 37 °C for 60 min. After being washed by PBS (pH = 7) for three times, the sponges were fixed by glutaraldehyde (2.5%) for another 2 h. Finally, sponges were gradually dehydrated using different concentrations of ethanol solution. The blood cells or platelet adhesion on the surface of dried sponges were observed by using SEM.

2.15. In vivo hemostatic performance

The prepared sponges' hemostatic ability was evaluated by a SD rat liver trauma model. Here, a hole punch was used to form a cylindrical wound with a diameter of 1 mm on the anesthetized rat liver. The pre-weighed gauze and sponges were immediately applied to the cylindrical wound, while the group with no treatment was used as the control group. And the prepared sponges' hemostatic ability was determined by the blood loss and the bleeding time.

2.16. In vivo wound repair performance

All animal studies were approved by the animal research committee of Sichuan University. Several healthy SD male rats (150 ± 20 g) were

acclimatized for 1 week. A certain amount of streptozotocin solution was injected into SD male rats (70 mg/kg) through the tail vein to induce diabetes mellitus type I [42–44]. After 3 days, 8 SD male rats (150 ± 20 g) with diabetes were used. After anesthesia, their backs were shaved and a round full-thickness skins with a diameter of 1.2 cm on the back of the rats were removed. In addition, wounds were infected with 100 μL of *S. aureus* suspension (1.0×10^8 CFU/mL). After 1 day, the wounds were treated with PBS, A-C, A-Ag, A-III, and A-Ag/III, respectively. For wound area monitoring, on the 2nd, 4th, 7th, 11th, and 14th day, the wound area was photographed. In order to evaluate epidermal regeneration and inflammation during wound repair process, samples collected on the 7th and 14th days were fixed with paraformaldehyde for 1 h and then stained with Hematoxylin-Eosin, Masson's Trichrome, CD68, CD31, and Ki67.

2.17. Statistical analysis

The mean ± standard deviation represented the results of statistical analysis of all experimental data. Student's *t*-test and chisquare test were applied to determine the statistical differences, and differences were considered significant if $P < 0.05$.

3. Results and discussion

3.1. Characterization of CMC/OS sponges with different MFC concentration

We proposed a novel method for the preparation of shape memory sponges involved introducing a porous three-dimensional (3D) polymer network structure, which was expected to be supplied by the Schiff base reaction between CMC containing $–NH_2$ and OS containing -CHO, and further structural reinforcement by the addition of MFC (Fig. 1). At First, the FT-IR spectrum of OS displaied an new stretching vibration band of -C = O appeared at 1738 cm^{-1} (Fig. S1), indicating the starch was successfully oxidized [45]. As illustrated in the TEM image of MFC suspension (Fig. S2), the MFC was displayed as nanoscale microfibrils with a large aspect ratio. By varying the concentration of the MCF suspension, CMC/OS-MFC sponges with different pore structures and mechanical properties were prepared by freeze-drying. As illustrated in Fig. S3, a new characteristic band appeared at 1637 cm^{-1} in the FT-IR spectrum of CMC/OS could be assigned to the formation of Schiff base bond (-C = N) [45]. And the SEM was conducted to investigate the microstructures of the CMC/OS-MFC sponges. As shown in Fig. 2A, the four sponges exhibited distinct porous structures. Due to the strong hydrogen bonding provided by MFC, CMC/OS-MFC sponges with high MFC contents displied small pore sizes and dense polymer networks. As we all know, this interconnected porous structure of the sponges was benificial for absorbing blood and excess exudation at the injured sites, decreasing the risk of bacterial infection, thus promoting wound repair [3,46].

In addition, porous natural polymer-based sponges possess the capability of fast water uptake [2]. The dynamic swelling behavior of the CMC/OS-MFC sponges was studied (Fig. 2B). Four sponges with different MFC content could quickly absorb water after being immersed into PBS (37 °C, pH = 7.4) and reach a swelling equilibrium within 20 min. And CMC/OS-$MFC_{0.2}$ sponge possessed the highest swelling ratio of 1953 ± 124%. CMC/OS-MFC_0, CMC/OS-$MFC_{0.4}$ and CMC/OS-$MFC_{1.2}$ showed lower swelling ratios of 1668 ± 137%, 1804 ± 134% and 1761 ± 101%, respectively. The addition of a small amount of hydrophilic MFC could enhance the porous structure and water retention of the sponges, thereby increasing their swelling rate. However, when the MFC content in the sponge precursor was further increased, the sponges' dry weight per unit volume and crosslink density were increased, resulting in a decrease of the swelling rate [2]. In conclusion, this excellent water absorption ability, on the one hand, would give the prepared sponge the capability to quickly absorb blood and excess wound exudate, thereby reducing the risk of bacterial infections, and be also conducive to concentrating the clotting factors and improve the speed of hemostasis [7].

Since the wound dressings are subject to the normal forces encountered during clinical use or handling [15], therefore, enough mechanical strength

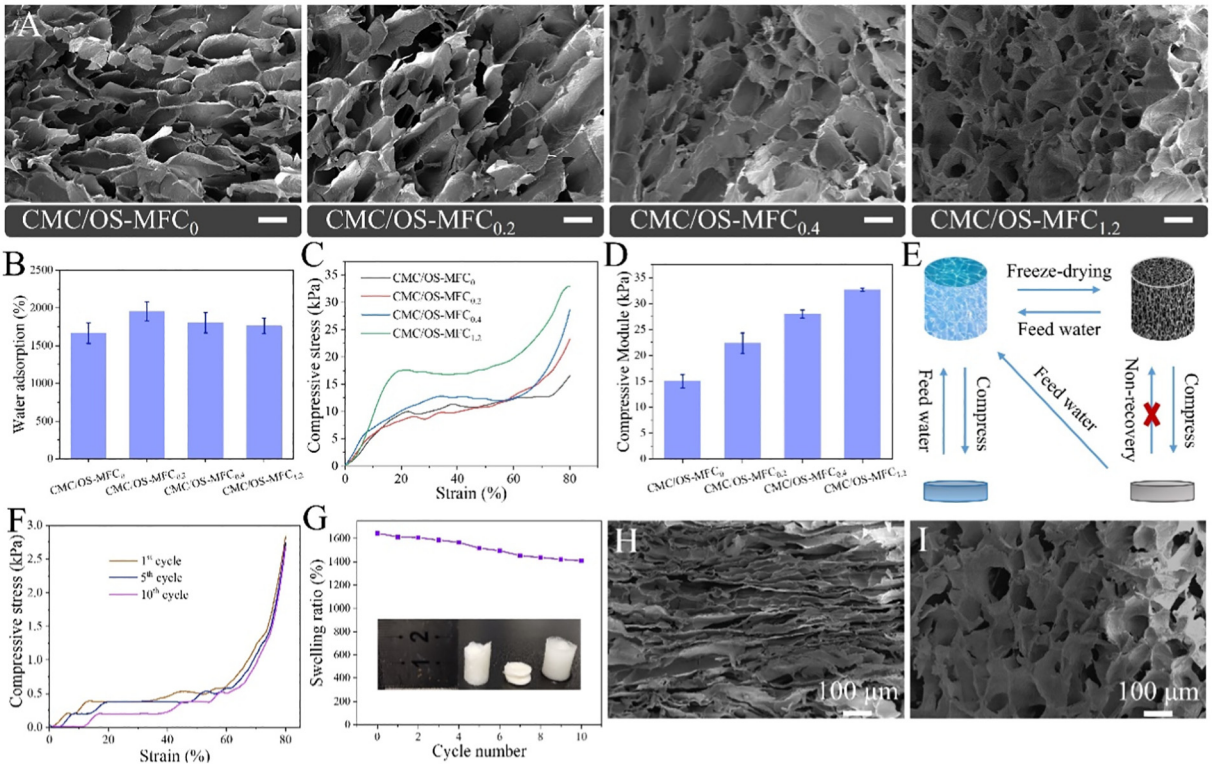

Fig. 2. The SEM images (A), swelling ratios (B), uniaxial compression stress – strain curves (C) and compressive module (D) of the CMC/OS sponges with MFC concentrations of 0, 0.2, 0.4, and 1.2 wt%. Scale bar: 200 μm. (E) Schematic illustration of the shape recovery mechanism. (F) The cyclic compression stress – strain curves of swollen CMC/OS-$MFC_{1.2}$ sponge. (G) Recyclability of the CMC/OS-$CMC_{1.2}$ sponge for the adsorption of PBS within 10 cycles. The inset was the picture of the sponge before and after compression and recovery shape by absorbing PBS. SEM images of CMC/OS-$MFC_{1.2}$ sponge in a compressed state (H), and recovered shape (I).

is the indispensable performance when sponges are applied in wound dressing [46]. However, the mechanical strength of the pure natural polymer-based macroporous sponge is generally weak, which may be detrimental to its clinical application [10]. We supposed that the addition of MFC with high aspect ratio could strengthen the mechanical performance of the sponges by further physically cross-linking the sponges' network. Herein, in order to assess the mechanical performance of the sponges with different MFC concentrations, the stress-strain test under 80% compression strain was conducted. As illustrated in Fig. 2C, the addition of MFC could significantly enhance the mechanical strength of CMC/OS-MFC sponge. As shown in Fig. 2D, with the increase of MFC concentration, the sponges' mechanical stress increased from 15.0 to 32.7 kPa, making it strong enough to sustain the swollen and expanded structure.

3.2. Water-/blood-triggered shape memory performance of CMC/OS-MFC$_{1.2}$ sponges

Hemostatic materials with shape memory function present distinctive virtue in hemostatic application because they can be delivered to wound through a syringe after being compressed, and restore their original geometry when in contact with blood to fill the abnormal wound boundaries and further stop blood loss [2,6,47]. The elastic porous structure, and excellent hydrophilicity of CMC/OS-MFC$_{1.2}$ sponge gave it the function of rapid water-triggered shape memory, indicating their potential in the application of preventing deep bleeding *via* serving as a physical barrier. Fig. 2E showed the schematic representation of the sponges' shape recovery mechanism.

This shape memory function of sponge was mainly ascribed to the reversible collapse of the porous structure in its hydrophilic matrix, allowing the liquid (including water or blood) to flow out/inflow freely. The shape recovery of squashed CMC/OS-MFC$_{1.2}$ sponges could be easily achieved by directly absorbing water within 3 s and the recovery ratio was nearly 100%, while sponges with lower MFC content did not have this water-triggered shape memory performance (Supplementary Movie 1). In addition to the water-triggered shape recovery phenomenon, the squashed CMC/OS-MFC1.2 sponge could quickly restore its original shape by absorbing blood after being injected into a glass bottle containing fresh blood (Supplementary Movie 2). In order to further assess the mechanical stability of the swollen sponges, a cyclic dynamic compression strain experience (80% strain, 10 cycles) was performed (Fig. 2F). The recovery loss of swollen sponges was small, indicating that the sponges exhibited excellent compressive elasticity at 80% compressive strain.

Fig. 2G showed the adsorption capacity of CMC/OS-MFC$_{1.2}$ sponges to PBS after the 10 drying-adsorption cycles. After each adsorption experiment was completed, the CMC/OS-MFC$_{1.2}$ sponges were freezing-dried. The adsorption capacity of CMC/OS-MFC$_{1.2}$ sponges did not decrease significantly after 10 cycles, and finally it was still 85% of the initial adsorption capacity. These results demonstrated the excellent structural stability and shape memory function of the CMC/OS-MFC$_{1.2}$ sponges. As illustrated in Fig. 2H and I, after being compressed to 80% strain, even if the pore structure of the sponge collapsed, the integrity of its network structure was basically maintained. Subsequently, the squashed sponge could quickly restore its primary porous structure after being fed with water. As demonstrated in Supplementary movie 3, the compressed sponge could recover its original shape by quickly adsorbing the squeezed out water after the load was removed. Thus, The CMC/OS-MFC$_{1.2}$ sponges with rapid blood-triggered shape recovery performance showed huge potential in hemostatic applications.

3.3. Characterization of AgNPs and rhCol III decorated sponges

Subsequently, the functional sponges were prepared by loading with AgNPs and rhCol III. Firstly, the UV − vis spectra of the CMC/$AgNO_3$ + TA suspension displayed a obvious absorption peak at 395.6 nm (Fig. 3A), which was attributed to the strong surface plasmon resonance transition peak of AgNPs. In addition, the XPS was used to confirm the

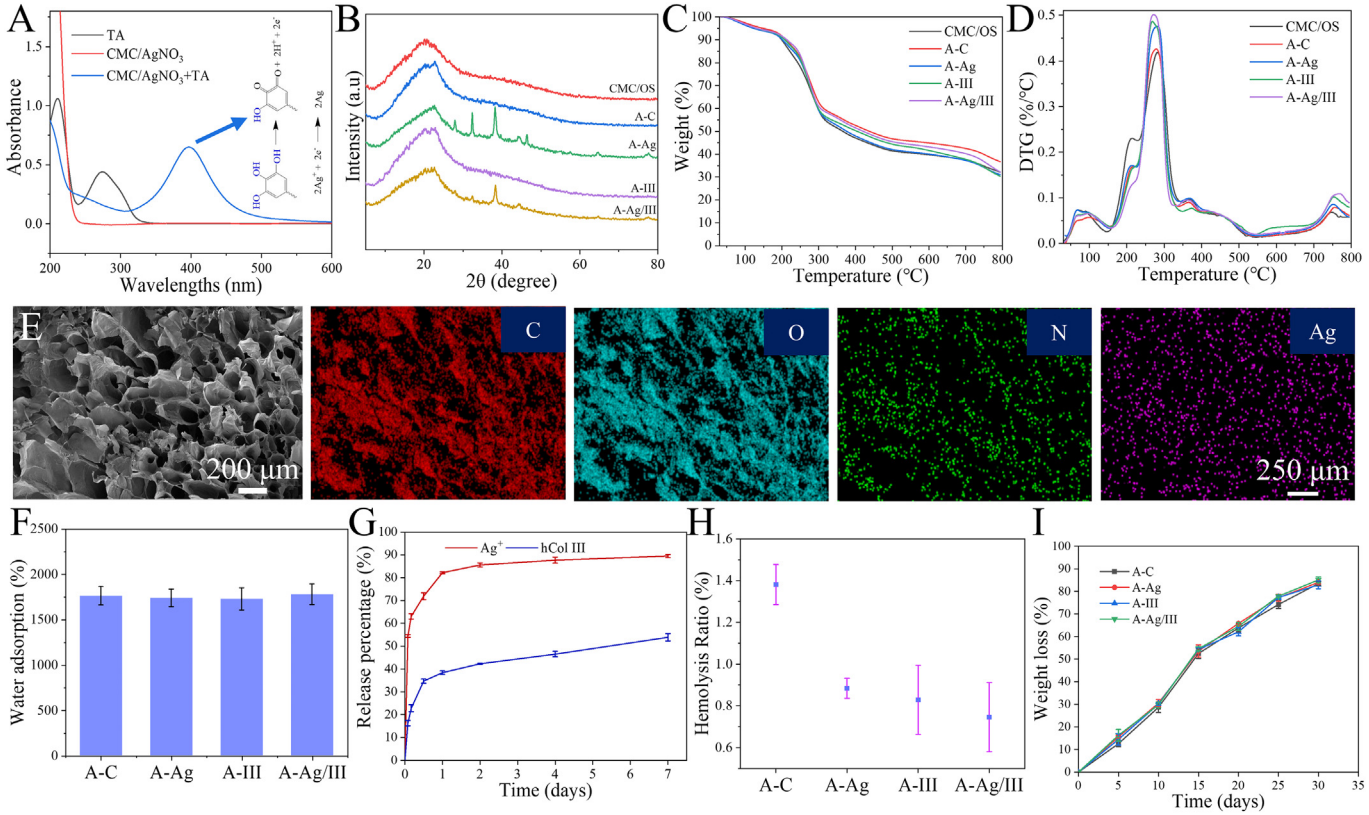

Fig. 3. (A) UV-vis spectra of TA, CMC/$AgNO_3$, and CMC/$AgNO_3$ + TA suspensions. Wide-angle XRD patterns (B), TGA curves (C) and DTG curves (D) of CMC/OS, A-C, A-Ag, A-III, and A-Ag/III. (E) SEM images and silver element SEM-mapping of A-Ag/III. (F) swelling ratios of A-C, A-Ag, A-III, and A-Ag/III in PBS at 37 °C. (G) Cumulative release profiles of Ag^+ and rhCol III from A-Ag/III in PBS. (H) The sponges' hemolytic percentage. (I) *In vitro* degradation kinetics of sponges in PBS.

presence of metallic silver in sponges. As illustrated in Fig. S4, two representative characteristic peaks with a binding energy difference of 6 eV at 367.5 eV and 373.5 eV were consistent with the binding energies of Ag $3d_{5/2}$ and Ag $3d_{3/2}$, respectively, illustrating the Ag was successfully generated in sponges [20]. And the new diffraction peaks in A-Ag and A-Ag/III at 38°, 44°, 64°, 77° and 81°, which were the XRD characteristic peaks of silver [48], further proved the successful synthesis of AgNPs (Fig. 3B).

For researching the thermal decomposition behavior of sponges, the TGA and DTG curves of sponges were presented in Fig. 3C and D, respectively. In the range of room temperature to 800 °C, the total weight loss of CMC/OS, A-C, A-Ag, A-III, and A-Ag/III were 67.83%, 63.27%, 68.96%, 69.67% and 67.74%, respectively (Fig. 3C). And results in Fig. 3D showed that the maximum thermal decomposition rates of CMC/OS, A-C, A-Ag, A-III, and A-Ag/III occured at 281 °C, 281 °C, 284 °C, 267 °C and 270 °C, respectively. After loading AgNPs and rhCOL III, there was no significant effect on the porous morphology of the sponge (Fig. 3E). Additionally, the partially enlarged SEM images of A-Ag/III clearly displayed AgNPs with uniform size were stably dispersed on the surface of the A-Ag/III (Fig. S5). The SEM mapping of the sponges (Fig. 3E and Fig. S6) further verified the uniform distribution of silver element in A-Ag and A-Ag/III. Moreover, results of Fig. 3F showed the swelling rate of A-Ag, A-III, and A-Ag/III was similar to that of A-C, ranging from 1727% to 1778%.

In order to prevent bacterial infections on the surface of chronic wounds, an effective solution is to place antibacterial materials that can release antibacterial agents continuously for a long time at the injured area. Consequently, to verify the antibacterial effect of A-Ag/III *in vitro*, we evaluated the sponges' release behavior of Ag^+ in PBS within seven days. As shown in Fig. 3G, in the first 24 h, there was a burst release of Ag^+ from A-Ag/III (over 80%), while the rate of Ag^+ release slowed down after 24 h (89.5% after 7 days). The bacteria in the injured site could be effectively killed by the early burst release of Ag^+ from A-Ag/III and then the slow release of Ag^+ could further inhibit the growth of bacteria. These above results indicated the A-Ag/III possessed an effective bactericidal effect and long-lasting antibacterial activity when applied to infected chronic wounds. Compared with Ag^+, rhCol III with a larger molecular weight was released more slowly. 38.4% of rhCol III was released in 24 h, and only 53.9% was released in 7 days.

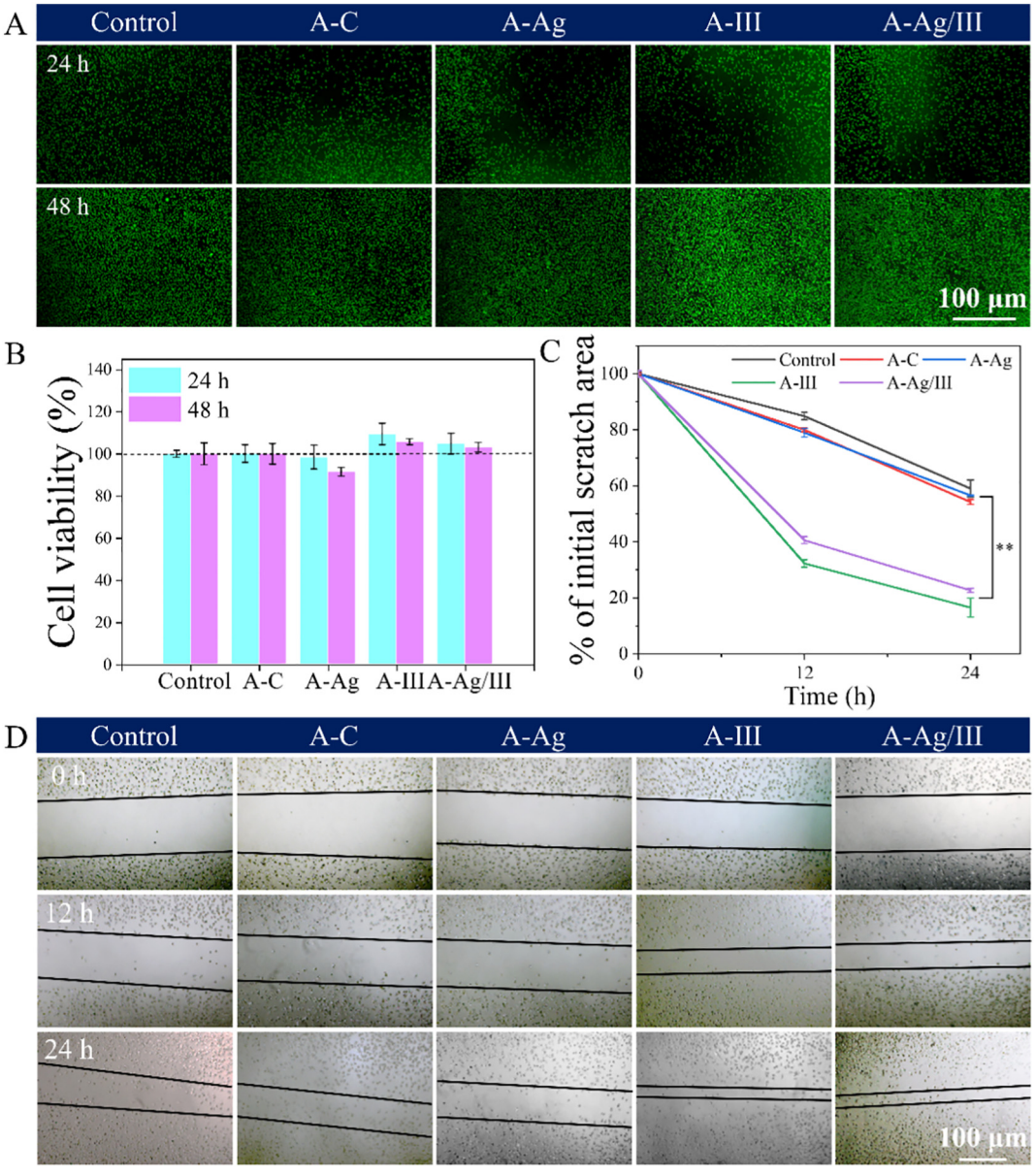

Fig. 4. (A) Live/Dead staining of L929 cells after incubated with sponges extract for 24 h. (B) Cytocompatibility evaluation of the sponges. Quantitative analysis (C) and images (D) of cell migration from the *in vitro* scratch assay. *$p < 0.05$, **$p < 0.01$.

3.4. Hemocompatibility, degradability and cytotoxicity effects of sponges

It is well known that the primary requirement of hemostatic materials is good hemocompatibility [8,20,46], what can be evaluated *in vitro* by the hemolysis assay [2]. As shown in Fig. S7, images from the hemolytic activity measurement showed that the clarity of the A-C, A-Ag, A-III, and A-Ag/III groups after centrifugation was similar to that of the DPBS group (transparent color), while the color of the Triton X-100 group was red. And the quantitative measurement results displayed these four sponges caused only 1.4%, 0.9%, 0.8% and 0.7% hemolysis, respectively (Fig. 3H), illustrating the prepared sponges possessed excellent hemocompatibility and huge potential in hemostatic field.

The *in vitro* degradation behavior of the A-C, A-Ag, A-III, and A-Ag/III was assessed by measuring weight loss of the sponges within a certain period of time in a simulated physiological environment. As illustrated in Fig. 3I, it was obvious that the weight of the four sponges gradually decreased over time. And the sponges in four groups degraded more than 70% after 20 days and almost completely degraded (> 80%) after one month in PBS. Therefore, these results suggested the prepared sponges were rapidly degradable material.

Low cytotoxicity and high biocompatibility are the basic requirements for the clinical application of biomaterials [2,20,49]. Therefore, in order to evaluate the cytocompatibility of sponges, the Live/Dead staining and CCK-8 assays were conducted [50]. As shown in Fig. 4A, most of L929

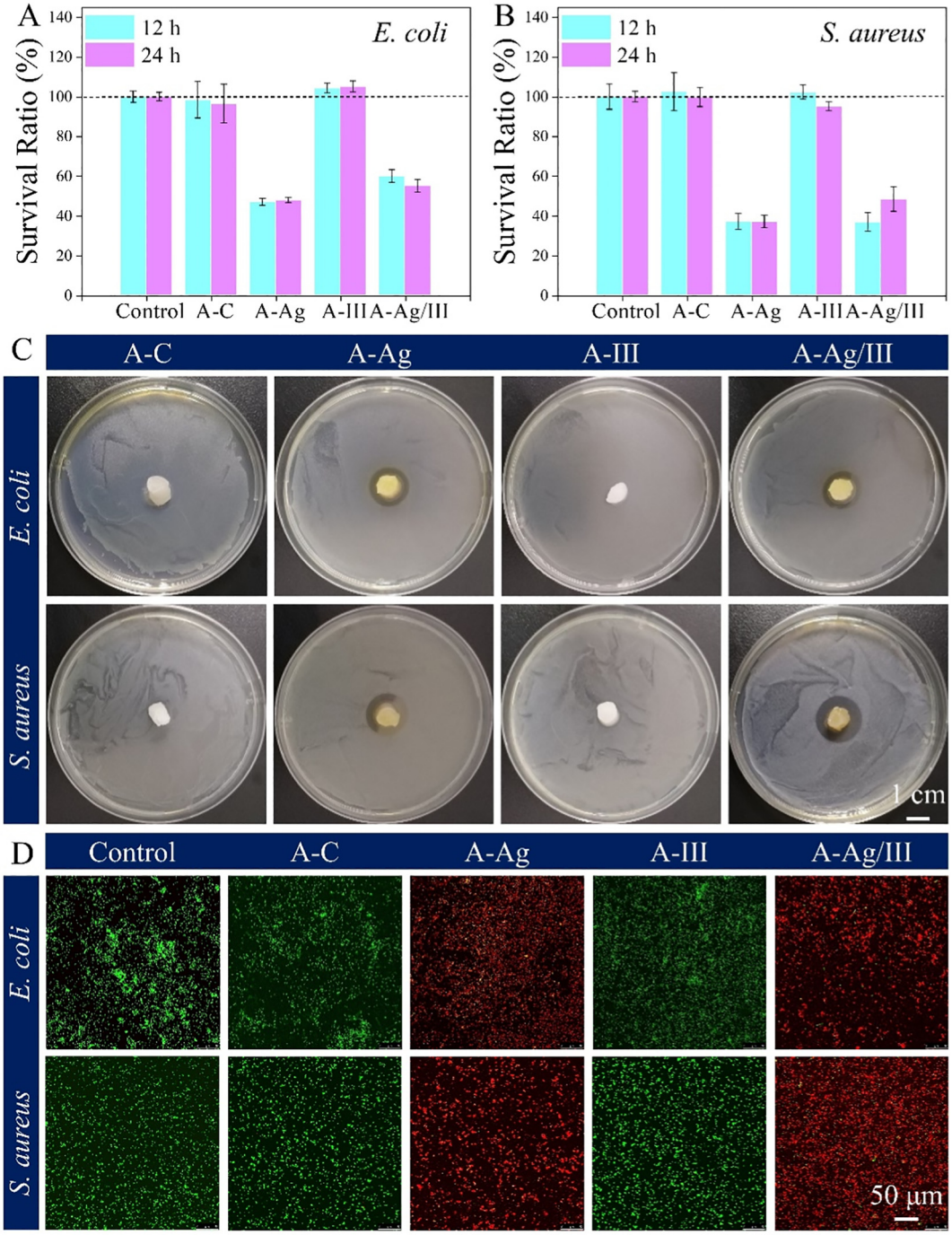

Fig. 5. Antibacterial performances of the four sponges against *E. coli* and *S. aureus*. OD600 values of *E. coli* (A) and *S. aureus* (B). (C) Inhibition zone diameter of the sponges. (D) The live/dead staining of bacteria after co-cultivating with sponges extract. Living bacteria exhibited green fluorescence, while dead bacteria exhibited red fluorescence.

cells in the four groups possessed a clear, well-extended and stretched morphologies, indicating the A-C, A-Ag, A-III, and A-Ag/III had no obvious influence on cells morphologies. Fig. 4B showed the cell viability of the four sponges was above 80%. The cell proliferation of A-Ag group was slightly inhibited by the release of Ag^{+}, while the sponges containing rhCol III with strong cell adhesion could promote cell proliferation.

The cell migration, like cell proliferation, is also a key procedure for effective tissue regeneration during the process of wound repair [51]. In order to demonstrate the function of the prepared sponges for enhancing the cell migration, *in vitro* wound scratch experiment was conducted. As illustrated in Fig. 4C and D, the scratched area in A-III and A-Ag/III groups decreased faster during 48 h of incubation than that in control group and the other sponges. As illustrated in Fig. 4C, the healing rate of cell scratch reached 83.4% and 77.3% after 48 h of incubation in A-III and A-Ag/III groups, respectively. While the control group, A-C, A-Ag only reached 41.0%, 45.8%, and 43.4%, respectively. The above results elucidated the rhCol III doped sponges possessed effective promotion effects on cell migration, making they a promising material for wound repair.

3.5. Antibacterial activity of the sponges

It is strongly recommended to employ the wound dressing with remarkable antibacterial activity to prevent infection-related serious issues which may result in various bacteremia reactions and even endanger human life [7,11,35,52]. Herein, classic etiological causes of soft tissue (especially skin) infections, including Gram-positive bacteria (*S. aureus*) and Gram-negative bacteria (*E. coli*) were selected to evaluate the antibacterial activity of sponges. Five different groups involved Control (negative control; no treatment), A-C, A-Ag, A-III, and A-Ag/III were tested for antibacterial activity. Results of the time-kill experiments conducted at pre-set time intervals indicated the well bactericidal effect in the A-Ag and A-Ag/III groups for *S. aureus* and *E. coli* (Fig. 5A and B). Then, as shown in Fig. 5C, results of zone inhibition assay displayed large inhibition zones for both *E. coli* and *S. aureus* in the A-Ag and A-Ag/III groups, which further verified the good antibacterial effect of AgNPs-doped sponges. In addition, the bacteria treated with four sponges were stained, here the live bacteria were stained fluorescent green and the dead bacteria were stained fluorescent red, and further observed with a fluorescence microscope. As illustrated in Fig. 5D, most of the *E. coli* and *S. aureus* in the control, A-C, and A-III groups were green (alive) and only a few bacteria (<0.5%) were red (dead). While the A-Ag and A-Ag/III treated *S. aureus* and *E. coli* were almost dead. These results demonstrated A-Ag and A-Ag/III sponges could induce the death of *S. aureus* and *E. coli*.

3.6. Hemostatic assay of sponges in vitro and in vivo

As the initial procedure during the wound repair process, hemostasis is a very critical step to avoid excessive blood loss before the beginning of the

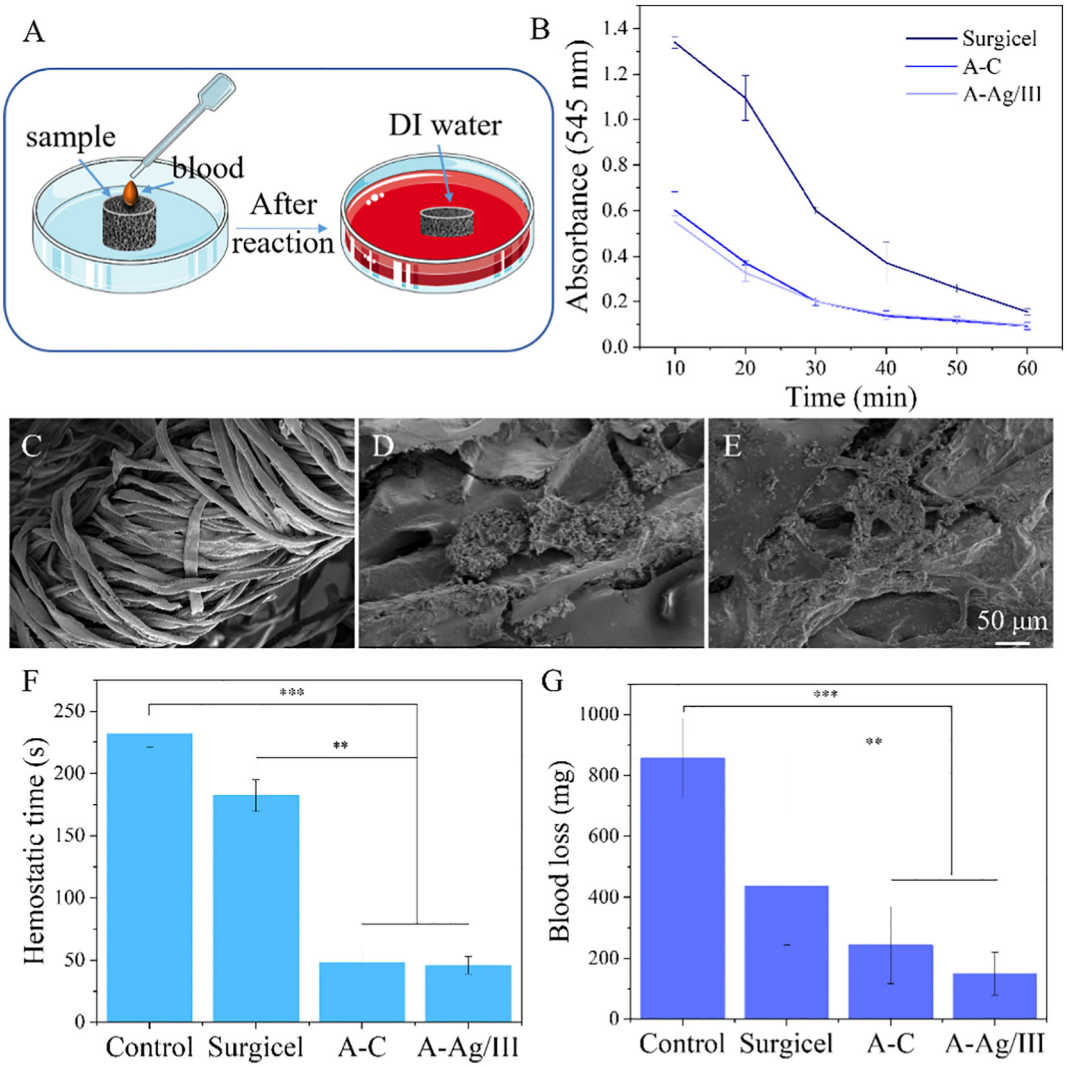

Fig. 6. (A) Schematic presentation of the whole blood clotting assay *in vitro*. (B) Dynamic whole-blood clotting assay of the sponges *in vitro*. SEM pictures of erythrocyte adhesion to the gauze (C), A-C sponge (D), and A-Ag/III sponge (E). Time to hemostasis (F) and blood loss (G) of the sponges in a rat liver trauma model.

intricate repair mechanisms of cells proliferation and tissue regeneration (maturation) [53]. The ideal wound repair process should start with stimulating the accumulation of platelets in the woud site and the formation of blood clots for hemostasis [8]. Herein, the whole blood clotting assay was conducted to evaluate the thrombogenicity and pro-coagulative performances of the prepared sponges [15]. Fig. 6A displayed the schematic graph of the whole blood clotting assay. Fresh blood was dropped directly on the surface of sponges, and deionized water was used to release free hemoglobin from erythrocytes in the uncoagulated blood at preset time intervals. As illustrated in Fig. 6B, at each time point, the whole blood clotting of A-C and A-Ag/III groups was remarkably higher than that of Surgicel gauze. These results demonstrated the prepared sponges possessed excellent blood-clotting capability, whereas the addition of AgNPs or rhCol III had no obvious effect. By means of observing the morphology of erythrocytes adhering to the surface of the sponge, the hemostatic mechanism of the sponge was further investigated. As displayed in Fig. 6C-E, only a small amount of erythrocytes adhesion could be observed on the surface of Surgicel, while numerous erythrocytes adhered on the surface of A-C and A-Ag/III.

Moreover, the hemostatic time and blood loss in a rat liver trauma model were recorded for the purpose of further investigating the blood-clotting property of sponges (Fig. S8). The volume of blood loss in the A-C and A-Ag/III groups was significantly less than that in the control and Surgicel groups. As shown in Fig. 6F, in the A-C and A-Ag/III groups, the time to hemostasis were 46 and 48 s, respectively, which were significantly faster than the control group (231 s) and Surgical gauze (132 s). In addition, the overall trend of the time to hemostasis was similar to the total blood loss (Fig. 6G). The volume of blood loss in the A-C group and A-Ag/III group were 243 and 150 mg, respectively. And the blood loss of the control group and the Surgicel group were 857 and 436 mg, respectively. These above results demonstrated that the hemostatic efficiency of sponge was better than that of commercial Surgicel, which might be attributed to the cationic CMC. The $–NH_2$ on the CMC molecular chain were protonated to $-NH3^+$ when in contact with blood, which would cause the erythrocyte adhesion and aggregation at the wound site through rapid electrostatic interaction with the negatively charged erythrocyte cell membrane [15]. In addition, the sponges with porous structure and high swelling capacity

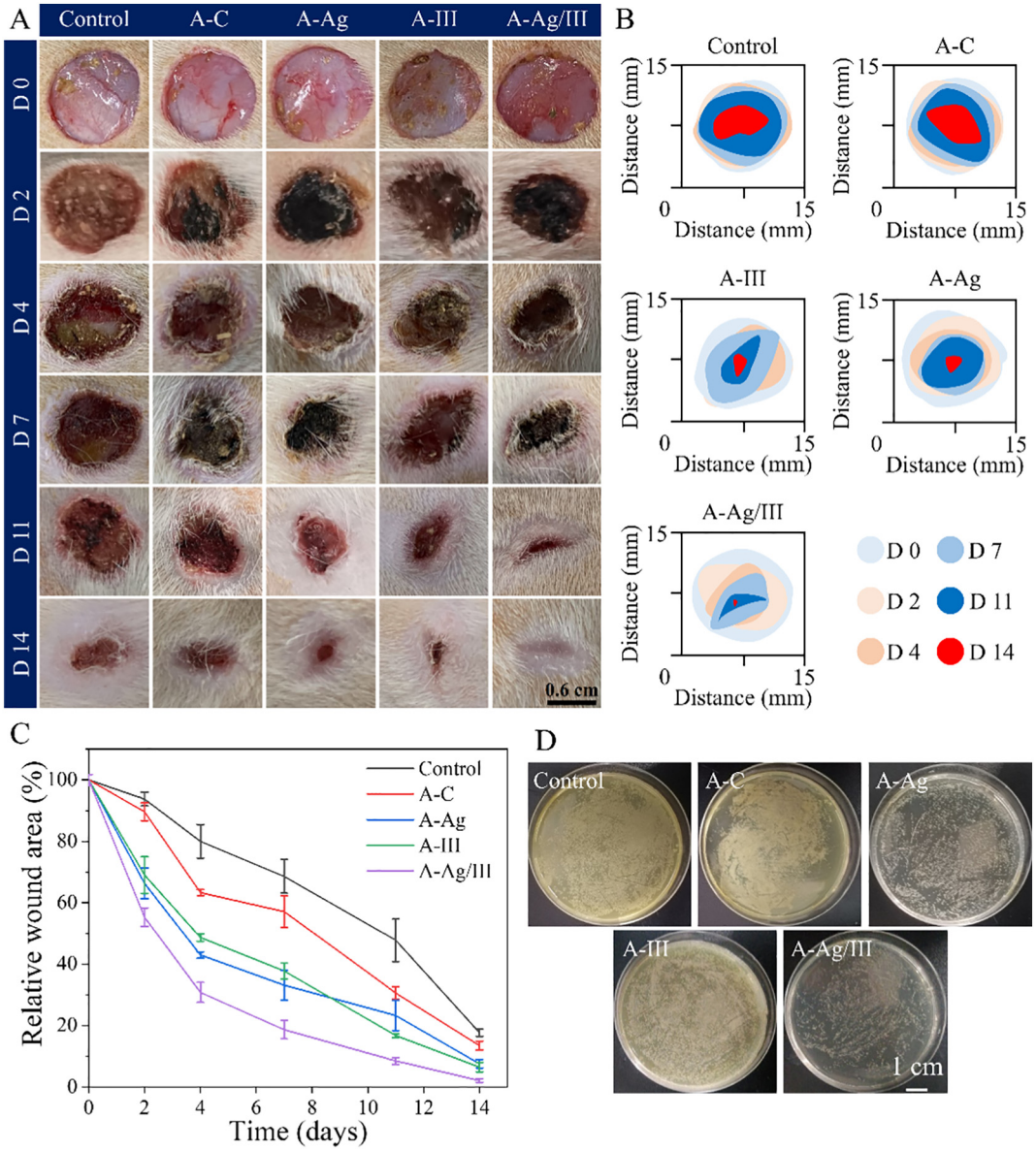

Fig. 7. (A) Representative images of the wound treated with control, A-C, A-Ag, A-III, and A-Ag/III on days 0, 2, 4, 7, 11, and 14. Traces of wound-bed closure (B) and wound contraction (C) during 14 days for each treatment. (D) Pictures of *S. aureus* colonies growing on the agar plates derived from the homogenized infected wounds after various treatments at 7 days.

could facilitate erythrocytes adhesion and aggregation, and activate the intrinsic coagulation pathway to promote the blood coagulation [21].

3.7. In vivo wound repairing efficacy

For chronic wound that can not be effectively therapied for a long time, multifunctional hemostatic materials should be capable of accelerating wound repair [1,54]. Herein, to evaluate the therapeutic effects of prepared sponges on chronic wound repair, the infected full-thickness wound model in the diabetic SD rat was established.

After application of sponges, the condition of wound repair was evaluated on day 0, 2, 4, 7, 11, and 14. As shown in Fig. 7A, wounds treated with A-C, A-Ag, A-III, and A-Ag/III displayed a faster healing rate than the control group. This might be attributed to the sponges possess inherent good blood/biocompatibility, biodegradability and rapid hemostasis, *etc.* For visualizing the change trend of wound area, wound trace pictures were drawn using ImageJ and PowerPoint softwares (Fig. 7B). As shown in Fig. 7C, the wound area of rat in A-Ag/III group decreased to 31% on day 7, which was significantly lower than that in control (80%), A-C (63%), A-Ag (43%), and A-III (49%) groups. After 11 d of treatment, the wound treated with A-Ag/III was decreased to 8%, whereas 47% and 31% of wounds remained in control and A-C groups, respectively. Moreover, on day 14, the wound treated with A-Ag/III showed a complete closure, but the A-C and the control groups still had wound area ratios of 13% and 17%, respectively. These results indicated the hemostatic A-Ag/III sponges could effectively stimulate infected wound repair. In addition, to evaluate the antibacterial ability of the prepared sponges *in vivo*, bacteria from wound tissues on day 7 were incubated on LB agar plates (Fig. 7D). Compared to the control group, the number of surviving

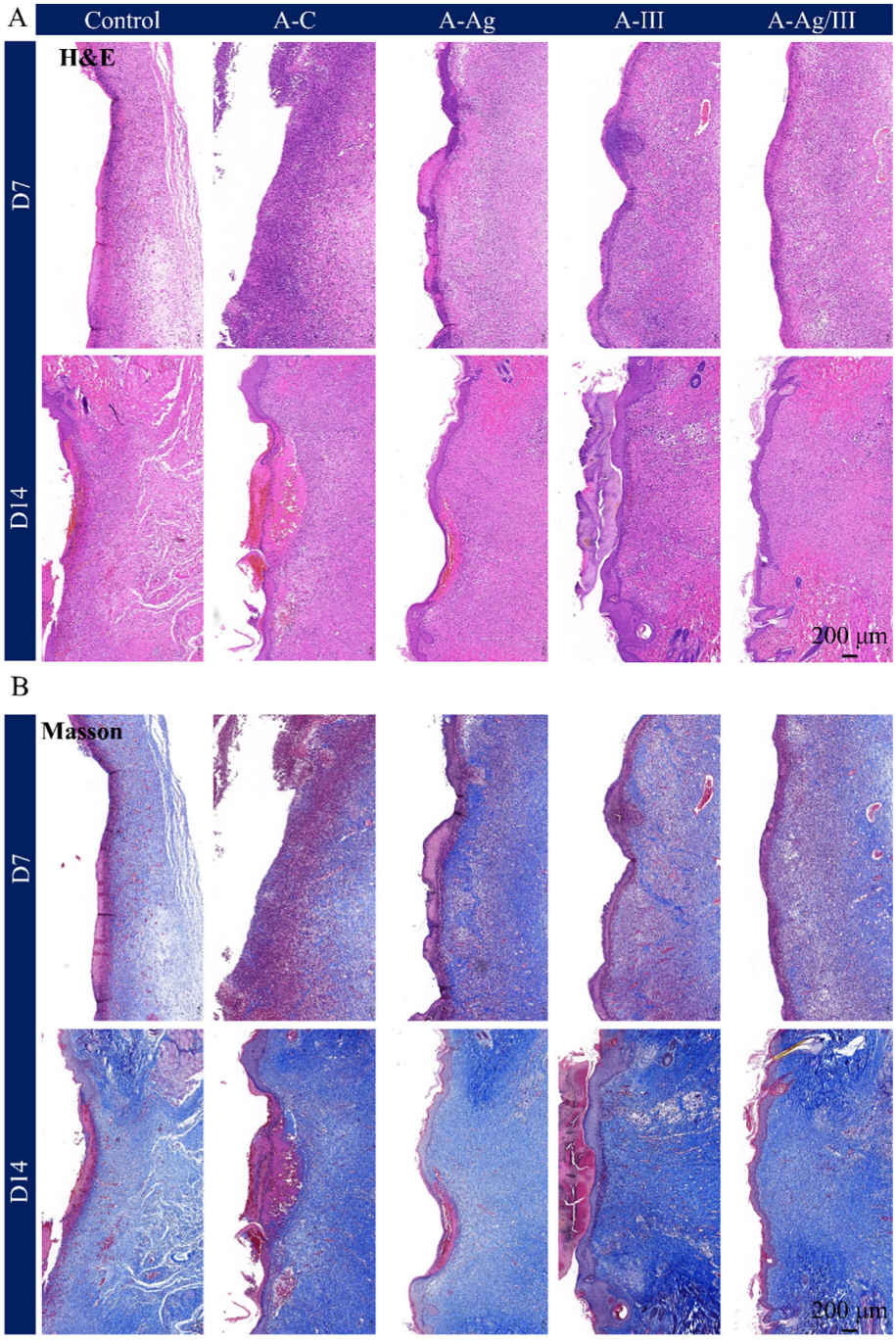

Fig. 8. H&E and Masson's staining of wound tissues at 7 and 14 days.

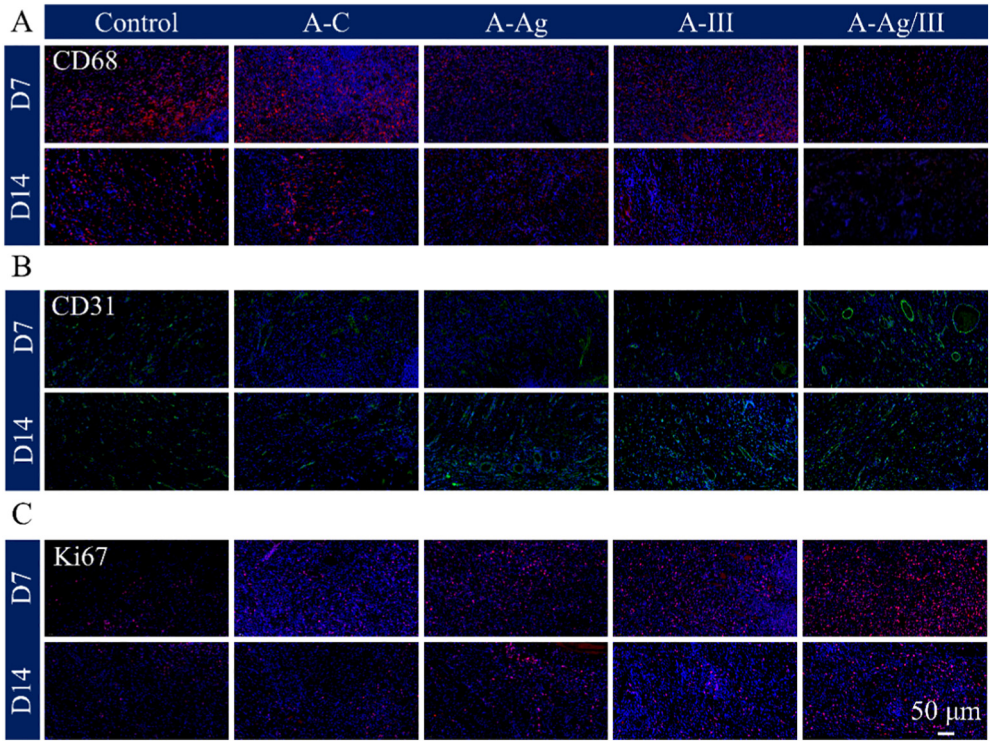

Fig. 9. Immunofluorescence staining of the wound-repairing assay. CD68 (red, A), CD31 (green, B) and Ki67 (red, C).

bacteria decreased to 92% (for A-C), 26% (A-Ag), 87% (A-III), 31% (A-Ag/III), revealing an excellent anti-infection activity of AgNPs decorated sponges *in vivo*. These results demonstrated the A-Ag/III sponges could accelerate wound healing by eliminating bacterial infections.

3.8. Histological analysis

Herein, the histological analysis was employed to further clarify the therapeutic effects of the prepared sponges on chronic wound repair. Specifically, on the 7th and 14th days, the skin samples were collected from the wound site and hematoxylin and eosin (H&E) staining was conducted for histomorphological examination. As illustrated in Fig. 8A, after receiving 7 days of treatment, the inflammatory cells in the A-Ag/III group were significantly less than those in the control and other sponges groups. In addition, a complete re-epithelium occurred in the wounds treated with A-Ag/III, while no new epithelial tissue was observed in the A-C and control groups. After receiving 14 days of treatment, the connective tissue remodeling and arrangement in A-Ag/III group was significantly better than those in the other groups. However, on the 14th day, there were still numerous inflammatory cells in the control group, indicating that the epidermis was not completely healed [54].

The amount of collagen deposition during wound healing was determined by Masson's staining (stained blue) [54,55]. On the 7th day, the collagen fibers stained blue were relatively dense in the A-Ag/III group, indicating that the skin tissue repair was active. On the 14th day, the A-Ag/III group displayed denser deposition of granulation tissue and better collagen bundles, as illustrated by blue staining in Fig. 8B. On the contrary, there were only poorly-developed shattered collagen bundles and small blue dyeing areas in the A-C and the control groups. These results indicated the A-Ag/III could serve as excellent wound dressing to prevent wound infection and accelerate wound repair after effective hemostasis application.

3.9. The expression of CD68, CD31 and Ki 67 in vivo

Persistent inflammation is the main reason why chronic wounds are difficult to repair, and alleviating the long-term inflammation has been proven to be an effective strategy to improve wound repair efficiency. CD68 is commonly found in macrophages and monocytes, especially near wounds [12]. The immunofluorescence staining of CD68 (Fig. 9A) displayed the expression level of CD68 was higher in the control and A-C groups than that in A-Ag/III group after reciving 7 days of treatment. On the 14th day, compared to other groups, the A-Ag/III group dispalyed the lowest CD68 expression, indicating the antibacterial A-Ag/III sponges could effectively inhibit the inflammatory response at the wound site.

Angiogenesis is critical to chronic wound repair as the blood vessels supply progenitor cells, nutrients and oxygen to maintain the cells proliferation and tissues remodeling [56,57]. CD31 has been widely used to investigate the neovascularization during wound repair [12,57]. The immunofluorescence staining of CD31 was displayed in Fig. 9B. Compared to the control and A-C groups, more CD31 expression could be observed in the wounds treated with A-Ag/III on the 7th day. Moreover, on the 14th day, the expression level of CD31 in the A-Ag/III group was remarkably higher than that in the control and A-C groups, indicating the A-Ag/III sponges could effectively promote vascular regeneration during wound repair process.

Ki67 is the upregulation of cell proliferation biomarkers [56,58]. During the process of wound repair, various kinds of cells were involved at different stages, including keratinocytes, endothelial cells, fibroblasts, inflammatory cells, *etc.* [56], which were labeled by immunofluorescence staining for Ki67 in this paper. As indicated in Fig. 9C, positive Ki67 cell number in the A-Ag/III group was remarkably higher than that in control and A-C groups at 7 and 14 days post-injury, suggesting that A-Ag/III could facilitate the cell proliferation during the repairing process, thereby accelerating the granulation tissue formation and enhancing collagen deposition [59]. In conclusion, by decreasing the expression of CD68 and simultaneously enhancing the expression of CD31 and Ki67, the hemostatic AgNPs and rhCol III loaded sponges could significantly promote wound repair.

4. Conclusion

Herein, a biodegradable, antibacterial and hemostatic A-Ag/III sponge was successfully fabricated through the Schiff bond reaction between CMC and OS with the reinforcement of MFC to achieve rapid hemostasis

and simultaneously promote wound repair. Due to their high porosity and complex interconnected porous structure, the prepared sponges could effectively adsorb abundant wound exudate to reduce the risk of infection and promote wound repair. In addition, the MFC-reinforced sponges could quickly recover their original shape by adsorbing water or blood after 80% compressive strain. And the macro/microstructure and mechanical properties of the swollen sponges would not suffer significant damage after 10 cycles. This water/blood-triggered shape memory function gave A-Ag/III great potential in dealing with deep, irregular, and incompressible bleeding. Both *in vitro* and *in vivo* hemostasis experiments demonstrated the A-Ag/III possessed rapid and efficient hemostasis property due to its excellent blood absorption capacity and the interaction between the amino groups of CMC and blood cells. Moreover, the A-Ag/III exhibited good biocompatibility and hemocompatibility, had broad-spectrum sterilization ability against *E. coli* and *S. aureus*, and the ability to promote proliferation and migration of L929 cells. The *in vivo* diabetic rat infected wound model demonstrated the A-Ag/III could promote wound repair by inhibiting inflammation, promoting cell proliferation, collagen deposition, and angiogenesis, revealing that this novel and multifunctional sponge possessed great application potential in hemostasis and wound dressing.

Supplementary data to this article can be found online at https://doi.org/10.1016/j.msec.2022.112669.

CRediT authorship contribution statement

Linyu Long and Cheng Hu: Experiments, Methodology, Software, Data processing and Writing–original draft; Wenqi Liu: Data illustration; Can Wu: Experiment assistance; Lu Lu: Animal-experiment direction; Yunbing Wang: Data curation and Writing–review & editing; Li Yang: Funding acquisition, Project administration, and Writing–review & editing.

Declaration of competing interest

The authors declare that they have no known competing financial interests or personal relationships that could have appeared to influence the work reported in this paper.

Acknowledgment

This work is supported by National Natural Science Foundation of China (32101107), National Key Research and Development Programs (2017YFC1104200), the Program of Introducing Talents of Discipline to Universities (111 Project, No. B16033), the Fundamental Research Funds for the Central Universities (No. YJ2021115) and the 135 project for disciplines of excellence, West China Hospital, Sichuan University (ZYJC21026, ZYJC21077).

References

[1] C. Cao, N. Yang, Y. Zhao, D. Yang, Y. Hu, D. Yang, X. Song, W. Wang, X. Dong, Biodegradable hydrogel with thermo-response and hemostatic effect for photothermal enhanced anti-infective therapy, Nano Today 39 (2021), 101165, https://doi.org/10.1016/j.nantod.2021.101165.

[2] X. Zhao, B. Guo, H. Wu, Y. Liang, P.X. Ma, Injectable antibacterial conductive nanocomposite cryogels with rapid shape recovery for noncompressible hemorrhage and wound healing, Nat. Commun. 9 (2018) https://doi.org/10.1038/s41467-018-04998-9.

[3] L. Gao, J. Chen, W. Feng, Q. Song, J. Huo, L. Yu, N. Liu, T. Wang, P. Li, W. Huang, A multifunctional shape-adaptive and biodegradable hydrogel with hemorrhage control and broad-spectrum antimicrobial activity for wound healing, Biomater. Sci. 8 (2020) 6930–6945, https://doi.org/10.1039/d0bm00800a.

[4] G. Thrivikraman, S.K. Boda, B. Basu, Unraveling the mechanistic effects of electric field stimulation towards directing stem cell fate and function: a tissue engineering perspective, Biomaterials 150 (2018) 60–86, https://doi.org/10.1016/j.biomaterials.2017.10.003.

[5] C. Liu, X. Liu, C. Liu, N. Wang, H. Chen, W. Yao, G. Sun, Q. Song, W. Qiao, A highly efficient, in situ wet-adhesive dextran derivative sponge for rapid hemostasis, Biomaterials 205 (2019) 23–37, https://doi.org/10.1016/j.biomaterials.2019.03.016.

[6] T.L. Landsman, T. Touchet, S.M. Hasan, C. Smith, B. Russell, J. Rivera, D.J. Maitland, E. Cosgriff-Hernandez, A shape memory foam composite with enhanced fluid uptake and bactericidal properties as a hemostatic agent, Acta Biomater. 47 (2017) 91–99, https://doi.org/10.1016/j.actbio.2016.10.008.

[7] Y. Fang, Y. Xu, Z. Wang, W. Zhou, L. Yan, X. Fan, H. Liu, 3D porous chitin sponge with high absorbency, rapid shape recovery, and excellent antibacterial activities for non-compressible wound, Chem. Eng. J. 388 (2020), 124169, https://doi.org/10.1016/j.cej.2020.124169.

[8] Z. Ahmadian, A. Correia, M. Hasany, P. Figueiredo, F. Dobakhti, M.R. Eskandari, S.H. Hosseini, R. Abiri, S. Khorshid, J. Hirvonen, H.A. Santos, M.A. Shahbazi, A hydrogen-bonded extracellular matrix-mimicking bactericidal hydrogel with radical scavenging and hemostatic function for pH-responsive wound healing acceleration, Adv. Healthc. Mater. 10 (2021) 1–19, https://doi.org/10.1002/adhm.202001122.

[9] Z. Abdollahi, E.N. Zare, F. Salimi, I. Goudarzi, F.R. Tay, P. Makvandi, Bioactive carboxymethyl starch-based hydrogels decorated with cuo nanoparticles: antioxidant and antimicrobial properties and accelerated wound healing in vivo, Int. J. Mol. Sci. 22 (2021) 1–18, https://doi.org/10.3390/ijms22052531.

[10] S. Ye, L. Jiang, J. Wu, C. Su, C. Huang, X. Liu, W. Shao, Flexible amoxicillin-grafted bacterial cellulose sponges for wound dressing. In vitro and in vivo evaluation, ACS applMater. Interfaces 10 (2018) 5862–5870, https://doi.org/10.1021/acsami.7b16680.

[11] C. Wang, H. Niu, X. Ma, H. Hong, Y. Yuan, C. Liu, Bioinspired, injectable, quaternized hydroxyethyl cellulose composite hydrogel coordinated by mesocellular silica foam for rapid, noncompressible hemostasis and wound healing, ACS Appl. Mater. Interfaces 11 (2019) 34595–34608, https://doi.org/10.1021/acsami.9b08799.

[12] Y. Yang, Y. Liang, J. Chen, X. Duan, B. Guo, Mussel-inspired adhesive antioxidant antibacterial hemostatic composite hydrogel wound dressing via photo-polymerization for infected skin wound healing, Bioact. Mater. (2021) https://doi.org/10.1016/j.bioactmat.2021.06.014.

[13] L. Wang, X. You, C. Dai, T. Tong, J. Wu, Hemostatic nanotechnologies for external and internal hemorrhage management, Biomater. Sci. 8 (2020) 4396–4412, https://doi.org/10.1039/d0bm00781a.

[14] S.K. Das, T. Parandhaman, M.D. Dey, Biomolecule-assisted synthesis of biomimetic nanocomposite hydrogel for hemostatic and wound healing applications, Green Chem. 23 (2021) 629–669, https://doi.org/10.1039/d0gc03010d.

[15] H. Yuan, L. Chen, F.F. Hong, A biodegradable antibacterial nanocomposite based on oxidized bacterial nanocellulose for rapid hemostasis and wound healing, ACS Appl. Mater. Interfaces 12 (2020) 3382–3392, https://doi.org/10.1021/acsami.9b17732.

[16] X.X. Wang, Q. Liu, J.X. Sui, S. Ramakrishna, M. Yu, Y. Zhou, X.Y. Jiang, Y.Z. Long, Recent advances in hemostasis at the nanoscale, Adv. Healthc. Mater. 8 (2019) https://doi.org/10.1002/adhm.201900823.

[17] L. Wang, Y. Zhong, C. Qian, D. Yang, J. Nie, G. Ma, A natural polymer-based porous sponge with capillary-mimicking microchannels for rapid hemostasis, Acta Biomater. 114 (2020) 193–205, https://doi.org/10.1016/j.actbio.2020.07.043.

[18] H. Cheng, C. Li, Y. Jiang, B. Wang, F. Wang, Z. Mao, H. Xu, L. Wang, X. Sui, Facile preparation of polysaccharide-based sponges and their potential application in wound dressing, J. Mater. Chem. B 6 (2018) 634–640, https://doi.org/10.1039/c7tb03000b.

[19] Z. Chen, L. Han, C. Liu, Y. Du, X. Hu, G. Du, C. Shan, K. Yang, C. Wang, M. Li, F. Li, F. Tian, A rapid hemostatic sponge based on large, mesoporous silica nanoparticles and: N -alkylated chitosan, Nanoscale 10 (2018) 20234–20245, https://doi.org/10.1039/c8nr07865c.

[20] Z. Wu, W. Zhou, W. Deng, C. Xu, Y. Cai, X. Wang, Antibacterial and hemostatic thiol-modified chitosan-immobilized AgNPs composite sponges, ACS Appl. Mater. Interfaces 12 (2020) 20307–20320, https://doi.org/10.1021/acsami.0c05430.

[21] J. Li, X. Sun, K. Zhang, G. Yang, Y. Mu, C. Su, J. Pang, T. Chen, X. Chen, C. Feng, Chitosan/Diatom-biosilica aerogel with controlled porous structure for rapid hemostasis, Adv. Healthc. Mater. 9 (2020) 1–13, https://doi.org/10.1002/adhm.202000951.

[22] X. Li, H. Cheng, X. Huang, S. Li, R. Yang, J. Wang, X. Wang, Facile construction of Chitin/Graphene nanocomposite sponges for efficient hemostasis, ACS Sustain. Chem. Eng. 8 (2020) 18377–18385, https://doi.org/10.1021/acssuschemeng.0c04721.

[23] B. Duan, Y. Huang, A. Lu, L. Zhang, Recent advances in chitin based materials constructed via physical methods, Prog. Polym. Sci. 82 (2018) 1–33, https://doi.org/10.1016/j.progpolymsci.2018.04.001.

[24] A. Muxika, A. Etxabide, J. Uranga, P. Guerrero, K. de la Caba, Chitosan as a bioactive polymer: processing, properties and applications, Int. J. Biol. Macromol. 105 (2017) 1358–1368, https://doi.org/10.1016/j.ijbiomac.2017.07.087.

[25] M. Ashrafizadeh, M. Delfi, F. Hashemi, A. Zabolian, H. Saleki, M. Bagherian, N. Azami, M.V. Farahani, S.O. Sharifzadeh, S. Hamzehlou, K. Hushmandi, P. Makvandi, A. Zarrabi, M.R. Hamblin, R.S. Varma, Biomedical application of chitosan-based nanoscale delivery systems: potential usefulness in siRNA delivery for cancer therapy, Carbohydr. Polym. 260 (2021) https://doi.org/10.1016/j.carbpol.2021.117809.

[26] A. Verlee, S. Mincke, C.V. Stevens, Recent developments in antibacterial and antifungal chitosan and its derivatives, Carbohydr. Polym. 164 (2017) 268–283, https://doi.org/10.1016/j.carbpol.2017.02.001.

[27] S. Torkaman, H. Rahmani, A. Ashori, S.H.M. Najafi, Modification of chitosan using amino acids for wound healing purposes: a review, Carbohydr. Polym. 258 (2021), 117675, https://doi.org/10.1016/j.carbpol.2021.117675.

[28] D.H. Ngo, T.S. Vo, D.N. Ngo, K.H. Kang, J.Y. Je, H.N.D. Pham, H.G. Byun, S.K. Kim, Biological effects of chitosan and its derivatives, Food Hydrocoll. 51 (2015) 200–216, https://doi.org/10.1016/j.foodhyd.2015.05.023.

[29] M.B. Kaczmarek, K. Struszczyk-Swita, X. Li, M. Szczęsna-Antczak, M. Daroch, Enzymatic modifications of chitin, chitosan, and chitooligosaccharides, Front. Bioeng. Biotechnol. 7 (2019) https://doi.org/10.3389/fbioe.2019.00243.

[30] W. Wang, Q. Meng, Q. Li, J. Liu, M. Zhou, Z. Jin, K. Zhao, Chitosan derivatives and their application in biomedicine, Int. J. Mol. Sci. 21 (2020) https://doi.org/10.3390/ijms21020487.

[31] P. Makvandi, M. Ghomi, M. Ashrafizadeh, A. Tafazoli, T. Agarwal, M. Delfi, J. Akhtari, E.N. Zare, V.V.T. Padil, A. Zarrabi, N. Pourreza, W. Miltyk, T.K. Maiti, A review on advances in graphene-derivative/polysaccharide bionanocomposites: therapeutics,

pharmacogenomics and toxicity, Carbohydr. Polym. 250 (2020), 116952, https://doi.org/10.1016/j.carbpol.2020.116952.
[32] H. Ye, J. Cheng, K. Yu, In situ reduction of silver nanoparticles by gelatin to obtain porous silver nanoparticle/chitosan composites with enhanced antimicrobial and wound-healing activity, Int. J. Biol. Macromol. 121 (2019) 633–642, https://doi.org/10.1016/j.ijbiomac.2018.10.056.
[33] J.Y. Liu, Y. Li, Y. Hu, G. Cheng, E. Ye, C. Shen, F.J. Xu, Hemostatic porous sponges of cross-linked hyaluronic acid/cationized dextran by one self-foaming process, Mater. Sci. Eng. C. 83 (2018) 160–168, https://doi.org/10.1016/j.msec.2017.10.007.
[34] L. Yao, H. Gao, Z. Lin, Q. Dai, S. Zhu, S. Li, C. Liu, Q. Feng, Q. Li, G. Wang, X. Chen, X. Cao, A shape memory and antibacterial cryogel with rapid hemostasis for noncompressible hemorrhage and wound healing, Chem. Eng. J. (2021), 131005, https://doi.org/10.1016/j.cej.2021.131005.
[35] Q. Jiang, B. Luo, Z. Wu, B. Gu, C. Xu, X. Li, X. Wang, Corn stalk/AgNPs modified chitin composite hemostatic sponge with high absorbency, rapid shape recovery and promoting wound healing ability, Chem. Eng. J. 421 (2021), 129815, https://doi.org/10.1016/j.cej.2021.129815.
[36] X. Yao, X. Qi, Y. He, D. Tan, F. Chen, Q. Fu, Simultaneous reinforcing and toughening of polyurethane via grafting on the surface of microfibrillated cellulose, ACS Appl. Mater. Interfaces 6 (2014) 2497–2507, https://doi.org/10.1021/am4056694.
[37] Y. Li, H. Xiao, Y. Pan, L. Wang, Novel composite adsorbent consisting of dissolved cellulose Fiber/Microfibrillated cellulose for dye removal from aqueous solution, ACS Sustain. Chem. Eng. 6 (2018) 6994–7002, https://doi.org/10.1021/acssuschemeng.8b00829.
[38] X. He, X. Fan, W. Feng, Y. Chen, T. Guo, F. Wang, J. Liu, K. Tang, Incorporation of microfibrillated cellulose into collagen-hydroxyapatite scaffold for bone tissue engineering, Int. J. Biol. Macromol. 115 (2018) 385–392, https://doi.org/10.1016/j.ijbiomac.2018.04.085.
[39] B. Lu, F. Lin, X. Jiang, J. Cheng, Q. Lu, J. Song, C. Chen, B. Huang, One-pot assembly of microfibrillated cellulose reinforced PVA-borax hydrogels with self-healing and pH-responsive properties, ACS Sustain. Chem. Eng. 5 (2017) 948–956, https://doi.org/10.1021/acssuschemeng.6b02279.
[40] D. Klemm, F. Kramer, S. Moritz, T. Lindström, M. Ankerfors, D. Gray, A. Dorris, Nanocelluloses: a new family of nature-based materials, Angew. Chemie - Int. Ed. 50 (2011) 5438–5466, https://doi.org/10.1002/anie.201001273.
[41] L. Yang, H. Wu, L. Lu, Q. He, B. Xi, H. Yu, R. Luo, Y. Wang, X. Zhang, A tailored extracellular matrix (ECM) - mimetic coating for cardiovascular stents by stepwise assembly of hyaluronic acid and recombinant human type III collagen, Biomaterials 276 (2021) https://doi.org/10.1016/j.biomaterials.2021.121055.
[42] C. Hu, F. Zhang, L. Long, Q. Kong, R. Luo, Y. Wang, Dual-responsive injectable hydrogels encapsulating drug-loaded micelles for on-demand antimicrobial activity and accelerated wound healing, J. Control. Release 324 (2020) 204–217, https://doi.org/10.1016/j.jconrel.2020.05.010.
[43] C. Hu, L. Long, J. Cao, S. Zhang, Y. Wang, Dual-crosslinked mussel-inspired smart hydrogels with enhanced antibacterial and angiogenic properties for chronic infected diabetic wound treatment via pH-responsive quick cargo release, Chem. Eng. J. 411 (2021), 128564, https://doi.org/10.1016/j.cej.2021.128564.
[44] C. Hu, W. Liu, L. Long, Z. Wang, Y. Yuan, W. Zhang, S. He, J. Wang, L. Yang, L. Lu, Y. Wang, Microenvironment-responsive multifunctional hydrogels with spatiotemporal sequential release of tailored recombinant human collagen type III for the rapid repair of infected chronic diabetic wounds, J. Mater. Chem. B 9 (2021) 9684–9699, https://doi.org/10.1039/d1tb02170b.
[45] Q. Mao, O. Hoffmann, K. Yu, F. Lu, G. Lan, F. Dai, S. Shang, R. Xie, Self-contracting oxidized starch/gelatin hydrogel for noninvasive wound closure and wound healing, Mater. Des. 194 (2020), 108916, https://doi.org/10.1016/j.matdes.2020.108916.
[46] M. Li, Z. Zhang, Y. Liang, J. He, B. Guo, Multifunctional tissue-adhesive cryogel wound dressing for rapid nonpressing surface hemorrhage and wound repair, ACS Appl. Mater. Interfaces 12 (2020) 35856–35872, https://doi.org/10.1021/acsami.0c08285.
[47] L. Zheng, Q. Wang, Y.S. Zhang, H. Zhang, Y. Tang, Y. Zhang, W. Zhang, X. Zhang, A hemostatic sponge derived from skin secretion of Andrias davidianus and nanocellulose, Chem. Eng. J. 416 (2021), 129136, https://doi.org/10.1016/j.cej.2021.129136.
[48] J. Chen, L. Qiu, Q. Li, J. Ai, H. Liu, Q. Chen, Rapid hemostasis accompanied by antibacterial action of calcium crosslinking tannic acid-coated mesoporous silica/silver janus nanoparticles, Mater. Sci. Eng. C. 123 (2021), 111958, https://doi.org/10.1016/j.msec.2021.111958.
[49] Y. Huang, X. Zhao, Z. Zhang, Y. Liang, Z. Yin, B. Chen, L. Bai, Y. Han, B. Guo, Degradable gelatin-based IPN cryogel hemostat for rapidly stopping deep noncompressible hemorrhage and simultaneously improving wound healing, Chem. Mater. 32 (2020) 6595–6610, https://doi.org/10.1021/acs.chemmater.0c02030.
[50] X. Chen, C. Cui, Y. Liu, C. Fan, M. Xiao, D. Zhang, Z. Xu, Y. Li, J. Yang, W. Liu, A robust poly(: N-Acryloyl-2-glycine)-based sponge for rapid hemostasis, Biomater. Sci. 8 (2020) 3760–3771, https://doi.org/10.1039/d0bm00770f.
[51] Y. Hao, W. Zhao, L. Zhang, X. Zeng, Z. Sun, D. Zhang, P. Shen, Z. Li, Y. Han, P. Li, Q. Zhou, Bio-multifunctional alginate/chitosan/fucoidan sponges with enhanced angiogenesis and hair follicle regeneration for promoting full-thickness wound healing, Mater. Des. 193 (2020), 108863, https://doi.org/10.1016/j.matdes.2020.108863.
[52] M. Tavakolizadeh, A. Pourjavadi, M. Ansari, H. Tebyanian, S.J. Seyyed Tabaei, M. Atarod, N. Rabiee, M. Bagherzadeh, R.S. Varma, An environmentally friendly wound dressing based on a self-healing, extensible and compressible antibacterial hydrogel, Green Chem. 23 (2021) 1312–1329, https://doi.org/10.1039/d0gc02719g.
[53] Z. Xu, B. Liang, J. Tian, J. Wu, Anti-inflammation biomaterial platforms for chronic wound healing, Biomater. Sci. 9 (2021) 4388–4409, https://doi.org/10.1039/d1bm00637a.
[54] Z. Yang, R. Huang, B. Zheng, W. Guo, C. Li, W. He, Y. Wei, Y. Du, H. Wang, D. Wu, H. Wang, Highly stretchable, adhesive, biocompatible, and antibacterial hydrogel dressings for wound healing, Adv. Sci. 2003627 (2021) 1–12, https://doi.org/10.1002/advs.202003627.
[55] S.M. Andrabi, P. Singh, S. Majumder, A. Kumar, A compositionally synergistic approach for the development of a multifunctional bilayer scaffold with antibacterial property for infected and chronic wounds, Chem. Eng. J. 423 (2021), 130219, https://doi.org/10.1016/j.cej.2021.130219.
[56] Z. Zheng, M. Li, P. Shi, Y. Gao, J. Ma, Y. Li, L. Huang, Z. Yang, L. Yang, Polydopamine-modified collagen sponge scaffold as a novel dermal regeneration template with sustained release of platelet-rich plasma to accelerate skin repair: a one-step strategy, Bioact. Mater. 6 (2021) 2613–2628, https://doi.org/10.1016/j.bioactmat.2021.01.037.
[57] X. Zhao, L. Liu, T. An, M. Xian, J.A. Luckanagul, Z. Su, Y. Lin, Q. Wang, A hydrogen sulfide-releasing alginate dressing for effective wound healing, Acta Biomater. 104 (2020) 85–94, https://doi.org/10.1016/j.actbio.2019.12.032.
[58] Y. Cheng, Y. Li, S. Huang, F. Yu, Y. Bei, Y. Zhang, J. Tang, Y. Huang, Q. Xiang, Hybrid freeze-dried dressings composed of epidermal growth factor and recombinant human-like collagen enhance cutaneous wound healing in rats, front. BioengBiotechnol. 8 (2020) 1–12, https://doi.org/10.3389/fbioe.2020.00742.
[59] L. Zhou, H. Zheng, Z. Liu, S. Wang, Z. Liu, F. Chen, H. Zhang, J. Kong, F. Zhou, Q. Zhang, Conductive antibacterial hemostatic multifunctional scaffolds based on Ti3C2TxMXene nanosheets for promoting multidrug-resistant bacteria-infected wound healing, ACS Nano 15 (2021) 2468–2480, https://doi.org/10.1021/acsnano.0c06287.